Letters in Applied NanoBioScience
Open-Access Journal (ISSN: 2284-6808)

Article
Volume 15, Issue 1, 2026, 39
https://doi.org/10.33263/LIANBS151.039

Synthesis, Spectral, DFT Studies, Molecular Docking, and *InSilico* ADME Prediction of VO(IV) Complexes of Kojic Acid and β-diketoenolates

Pradeep Kumar Vishwakarma [1,*], Ram Charitra Maurya [1], Pushpendra Singh Jaget [1], Ashwani Kumar Sharma [1,2], Sutapa Roy [3], Ranjan Kumar Mohapatra [4], Lucia Pintilie [5]

1 Department of Chemistry and Pharmacy, Rani Durgavati Vishwavidyalaya, Jabalpur 482001, India
2 Department of Chemistry, Govt. Digvijay (Autonomous) Post-Graduate College, Rajnandgaon, India
3 Department of Chemistry, St. Aloysius College, Jabalpur 482001, India
4 Department of Synthesis of Bioactive Substances and Pharmaceutical Technologies, National Institute for Chemical & Pharmaceutical Research and Development, Bucharest, Romania
* Correspondence: pkvchemrduni1@gmail.com;

Received: 31.01.2024; Accepted: 30.06.2024; Published: 30.03.2026

Abstract: In this manuscript, we represent the synthesis, characterization, antibacterial activities, and theoretical studies (molecular docking and ADME) of VO(IV) complexes of kojic acid and substituted β-diketones. The molecular composition of the synthesized compounds [VO(ka)(L)(H_2O)], Where Hka= Kojic Acid, HL=β-diketones viz., methyl acetoacetate, ethyl acetoacetate, benzoyl acetone, or dibenzoyl methane, has been synthesized. The resulting complexes have been characterized by elemental analysis, vanadium determination, molar conductance and magnetic measurements, FT-IR, ESI-MS, and ESR. Then, computational analysis was done using Gaussian 09 software. These studies have suggested that monomeric distorted octahedron structures are suitable for these complexes. The proposed structures have been confirmed by examining bond lengths and bond angles for a representative compound, [VO(ka)(eacac)(H2O)] C2. Moreover, a molecular docking study was performed with human CYP3A4 bound to metformin (PDB ID: 5G5J) to evaluate the antioxidant activity, and with the ptp1b-inhibitor complex (PDB ID: 2QBS) to evaluate the antidiabetic activity. Finally, the *Insilco* ADME properties were done with the SwissADME online server.

Keywords: oxidovanadium(IV) complexes; DFT; ADME; molecular docking.

1. Introduction

The field of coordination chemistry is highly interested in 3-hydroxy-2-methyl-4H-pyrone-4-one (maltol) and 5-hydroxy-(2-hydroxymethyl)-4H-pyrone-4-one (kojic acid) as ligands [1]. Many species of Aspergillus, Acetobacter, and Penicillium produce H_2Ka, a fungal metabolite. The discovery was made during the investigation of the formation of steamed rice (Koji). Other food items that contained it included sake, miso (soybean paste), shoyu (soy sauce), and others. Kojic acid is produced on an industrial scale and added to food for its antibacterial and fungicidal properties [2]. Due to their flavoring and antioxidant properties, kojic acid, maltol, and ethyl maltol have been chosen for their use in food production [3]. Researchers have been interested in oxovanadium complexes because of their well-known biological actions[4,5]. Different ligands have been employed in the successful synthesis of

vanadium complexes with different oxidation states, and their magnetic properties, antidiabetic, anti-inflammatory, and catalytic activities have been evaluated [6,7]. The molecular geometry of the oxovanadium(IV) complex is significantly influenced by the chelating properties of the ligands, as evidenced by the published literature. Schiff bases are reported to form stable complexes with vanadium, primarily with coordination numbers of 4, 5, or 6 [8]. For four and five-coordinate complexes, square pyramidal, distorted square pyramidal, or distorted trigonal bipyramidal geometry have been reported, and for six-coordinated ones, distorted octahedral structures with the apical position occupied by an oxygen atom have been observed [9].

Given their wide applications, we aimed to design, synthesize, and characterize oxovanadium(IV) complexes with an O6 coordination environment involving kojic acid and substituted β-ketoenolates. After completing successful synthesis and experimentation, we analyzed theoretical chemistry using DFT, molecular docking, and ADME properties. Furthermore, antimicrobial screening was performed on these complexes.

2. Materials and Methods

2.1. Experimental

All chemicals used were of analytical reagent (AR) grade. Elemental analysis, X-band EPR spectrum was recorded at RT on an X-band ESR spectrometer using a powdered sample at a microwave frequency of 9.11 GHz, and TGA was performed by heating the sample at 10°C min^{-1} from 25 to 1000°C on a thermal analyzer from SAIF, IIT, Mumbai. Solid-state FT-IR spectra were obtained using potassium bromide pellets with a Perkin-Elmer model 1620 infrared spectrophotometer, and mass spectra were recorded from SAIF, CDRI Lucknow. The conductance measurements were made in dimethylformamide solution using a Toshniwal conductivity bridge and dip-type cell with a smooth platinum electrode of cell constant 1.02, and magnetic measurements were performed by Guoy's method with mercury(II) tetrathiocyanatocobaltate(II) as calibrant at SAIF, IIT, Chennai. The decomposition temperatures (DT) were recorded on a melting-point apparatus with a maximum heating capacity of 360°C. Electronic spectra were recorded on an ATI Unicam UV-2-100 UV/Visible spectrophotometer using a 1.0 cm silica cell, and electrochemistry was performed on a BASi Epsilon electrochemical analyzer with tetrabutylammonium tetrafluoroborate (TBATFB) as the supporting electrolyte.

2.2. Synthesis of mixed ligand complexes C1-C4.

To a solution of 5-hydroxy-2-(hydroxy methyl)-4-pyrone (kojic acid) (0.001 M; 0.142 g) in 10 mL of ethanol was added 0.001 M of methyl acetoacetate (0.116 g) or ethyl acetoacetate (0.130 g), benzoyl acetone (0.162 g), or dibenzoyl methane (0.224 g) in 10 mL of ethanol. The resulting mixture of the two appropriate ligands was added slowly, with constant stirring, to a solution of 0.001 M VOSO4·5H2O (0.253 g) in 1 mL of water and 10 mL of ethanol, and a dark green (aquamarine) solution was obtained after refluxing the mixture for ~4 hrs. Thereafter, an ammonium hydroxide solution (50%) was added dropwise to adjust the pH to 8, and thereby the solution turned a darker green. After 60 minutes of refluxing, the reaction mixture was collected by vacuum filtration, yielding a dark green and light brown precipitate. Ethanol-water (1:5) was used to wash it, and it was then dried overnight under vacuum.

[VO(ka)(macac)(H_2O)] **C1** Yield; 0.256g 75%, Colour; Light brown, decomposition temperature; 240°C, Anal. Calc. for $C_{11}H_{14}O_9V$ (MW: 341.18); C, 38.73; H, 4.14; V,14.93 Found: C, 38.70; H, 4.18 %. Solubility: DMF and DMSO. IR (KBr, 4000-600 cm^{-1}); *v*(C=O) 1597, *v*(C=C) 1565, *v*(C–O) 1280 and *v*(V=O) 972, and (H_2O) 3440 cm^{-1}, UV/Vis (DMSO) λ_{max} nm: 287, 300 and 393.

[VO(ka)(eacac)(H_2O)] **C2** Yield; 0.241 g 68 %, Colour; Light brown, decomposition temperature; 210°C, Anal. Calc. for $C_{12}H_{16}O_9V$ (MW: 355.21); C, 40.58; H, 4.54; V, 14.34. Found: C, 40.53; H, 4.51; V 14.36 %. Solubility: DMF and DMSO, IR (KBr, 4000-400 cm^{-1}); *v*(C=O) 1602, *v*(C=C) 1534, *v*(C–O) 1270, v(V=O) 986 and (H_2O) 3446 cm^{-1}, UV –Vis (DMSO) λ_{max} nm: 279, 307 and 380.

[VO(ka)(dbm)(H_2O)] **C3** Yield; 0.287 g 64%, Colour; Light green, decomposition temperature; 180°C, Anal. Calc. for $C_{21}H_{18}O_8V$ (MW:449.32); C, 56.14; H, 4.04; V, 11.34; Found: C, 56.33; H, 4.01; V, 10.96 %, Solubility: DMF and DMSO, IR (KBr, 4000-600 cm^{-1}); *v*(C=O) 1616, *v*(C=C) 1588, *v*(C–O) 1350, *v*(V=O) 974 and (H_2O) 3458 cm^{-1}, UV–Vis (DMSO) λ_{max} nm: 289,316 and 361.

[VO(ka)(bac)(H_2O)] **C4** Yield: 0.270 g 70%, Colour; Light green, decomposition temperature; 200°C, Anal. Calc. for $C_{16}H_{14}O_8V$ (MW:387.25); C, 56.14; H, 4.04; V, 11.34; Found: C, 56.21; H, 4.56; V, 11.23 % Solubility: DMF and DMSO, IR (KBr, 4000-600 cm^{-1}); *v*(C=O) 1708, *v*(C=N) 1627, *v*(C–O) 1350, *v*(C=S) 1135 *v*(V=O) 974 and (H_2O) 3399 cm^{-1}, UV–Vis (DMSO) λ_{max} nm: 270, 438 and 460.

2.3. Theoretical studies.

The theoretical chemistry was performed using the Gaussian 09 software package [10]. B3LYP/6-311+G and B3LYP/LANL2MB combinations are used to set up the DFT calculations. To understand the vibrational properties and structural characteristics of a representative studied compound. The assignment of the calculated wavenumbers was aided by the animation option in the graphical user interface of GaussView 9.0 for Gaussian programs, which provides a visual presentation of the shapes of the vibrational modes [11]. DFT at the B3LYP level has been utilized to verify the geometries. In addition, the quantum parameters indicate the potential bioactivity of the oxidovanadium(IV) compounds [12]. Visualized demonstrations of molecular electrostatic potentials (MEPs) reveal electrophilic/nucleophilic reactive sites, which support theoretical biological activities involving H-bonding interactions [13]. We present and discuss the molecular structures, vibrational frequencies, FMOs, and atomic charges that have been optimized for kojic acid and C2.

2.4. Molecular docking interactions.

In recent years, Molecular Docking has become a crucial part of in-silico drug development. The objective of this technique is to predict the interaction between a small molecule and a protein at the atomic level [14]. The molecular docking study was performed on five compounds (kojic acid and four complexes **C1-C4**) to obtain accurate predictions about the structure and interactions of the studied compounds in complex with a protein/enzyme receptor to evaluate the antioxidant and antidiabetic activity. For this study, the following two proteins/enzymes' receptors have been imported from the protein data bank (http://www.rcsb.org/:PDB): Crystal structure of human CYP3A4 bound to metformin (PDB

ID: 5G5J) [15] to evaluate the antioxidant activity. Crystal structure of the ptp1b-inhibitor complex (PDB ID: 2QBS) [16] to evaluate the antidiabetic activity.

The binding site on the protein/enzyme target's surface was fitted with the complex compounds studied during the docking simulation. The docking score and hydrogen bonds formed with amino acid residues in the receptor's active site are used to predict ligand binding modes, binding affinity, and ligand orientation within the receptor's active site [17,18]. The docking scores were compared with the score of kojic acid. The protein-ligand complex has been realized based on the X-ray structure of human CYP3A4 bound to metformin (PDB ID 5G5J) and on the X-ray structure of the ptp1b-inhibitor complex (PDB ID 2QBS).

2.5. Insilco ADME properties.

This is the third theoretical approach in the present investigation, which uses the evaluation of the ADME properties. This investigation is carried out to determine whether the studied compounds exhibit toxicity upon administration or have a pharmacokinetic profile. Proceeding for this purpose, Swiss ADME [19] servers were used. Based on the chemical structure, the desired compounds were characterized to predict their pharmacokinetic properties, such as absorption, distribution, metabolism, and elimination (ADME), as well as their pharmacodynamic potential and toxicity, to avoid potential interactions with off-targets that could cause many side effects.

3. Results and Discussions

The oxovanadium(IV) complexes were prepared by treating $VOSO_4 \cdot H_2O$ with kojic acid and substituting β-ketoenolates in aqueous ethanol, as shown in the following equations.

$$VOSO_4 + kaH + LH \xrightarrow[\text{Reflux}]{\text{Ethanol}, H_2O} [VO(ka)(L)(H_2O)] + H_2SO_4 \qquad (1)$$

Where H_2ka = kojic acid, HL = β-ketonolates like methyl acetoacetate (Hmacac), ethyl acetoacetate (Heacac), benzoyl acetone (Hbac), or dibenzoyl methane (Hdbm).

All the synthesized complexes are air-stable and color solid masses. The experimental section provides information on their thermal stability and decomposition temperatures. These are insoluble and sparingly soluble in organic solvents, but they are also soluble in DMF, DMSO, and acetonitrile. The formulation of these complexes can be confirmed by experimental studies, elemental analysis, magnetic measurements, and spectral analyses.

3.1. Spectral studies.

The experimental section presents the infrared spectral bands of kojic acid and its compounds, along with their likely assignments. The vibrational bands at 1700 and 1660 cm-1 are most likely due to the non-hydrogen-bonded and hydrogen-bonded carbonyl vibrational modes, respectively. When kojic acid forms a complex with the vanadium ion, the former mode disappears, and the latter shifts to lower frequencies and merges with ν(C=O) (acetyl/benzoyl) of β-diketone ligands used as co-ligands in the present investigation (vide infra). The strong bands appearing at 3220 and 3265 cm^{-1} are due to ν(OH) (phenolic) and ν(OH) of the CH_2OH group of the kojic acid. The ν(OH) (phenolic) disappears after complexation, and this suggests the coordination of phenolic oxygen after deprotonation with vanadium. This is further

supported by the upward shift of the free ν(C-O) phenolic of kojic acid, which appears in the range 1270-1287 cm^{-1} after complexation. The appearance of ν(OH) of the CH_2OH group of kojic acid at a bit lower frequency (3190-3200 cm^{-1}) indicates that the OH group of the CH_2OH moiety is inert towards coordination. These results conclude that kojic acid serves as a bidentate (O, O) chelating ligand. The illustrative absorption frequencies due to coordinated methyl acetoacetate, ethyl acetoacetate, benzoyl acetone, or dibenzoyl methane anions are ν(C=O) (acetyl/benzoyl) and ν(C=C) modes, and these have been observed in the region 1594-1616 and 1534-1588 cm^{-1}, respectively. Most of the VO(II) complexes show a strong band close to 1000 cm^{-1}, which has been assigned to the ν(V=O) [20]. In contrast, several VO(IV) complexes have been reported in which this stretching mode appears at quite lower wave numbers, around 900 cm^{-1} [21]. The shift of the ν(V=O) band to lower wavenumbers has been suggested due to the presence of a slight ···V=O···V=O··· type interaction occurs between one molecule's vanadyl oxygen and a vanadium metal in another molecule [22]. According to the present study, (V=O) is discovered at 972-993 cm^{-1}, indicating no interaction between V=O….V=O…V=O.. interaction in these complexes. All complexes exhibit a broad band in the infrared spectrum at 3399-3458 cm^{-1}. This suggests the presence of coordinated water molecules/lattice water molecules. An almost identical resemblance can be seen between the experimental and theoretical IR spectra of a representative complex, C2, and the important spectral bands in Figure 1. Supplementary Figures 1 and 2 depict the theoretical IR spectrum of Kojic acid and the experimental IR of C3, respectively.

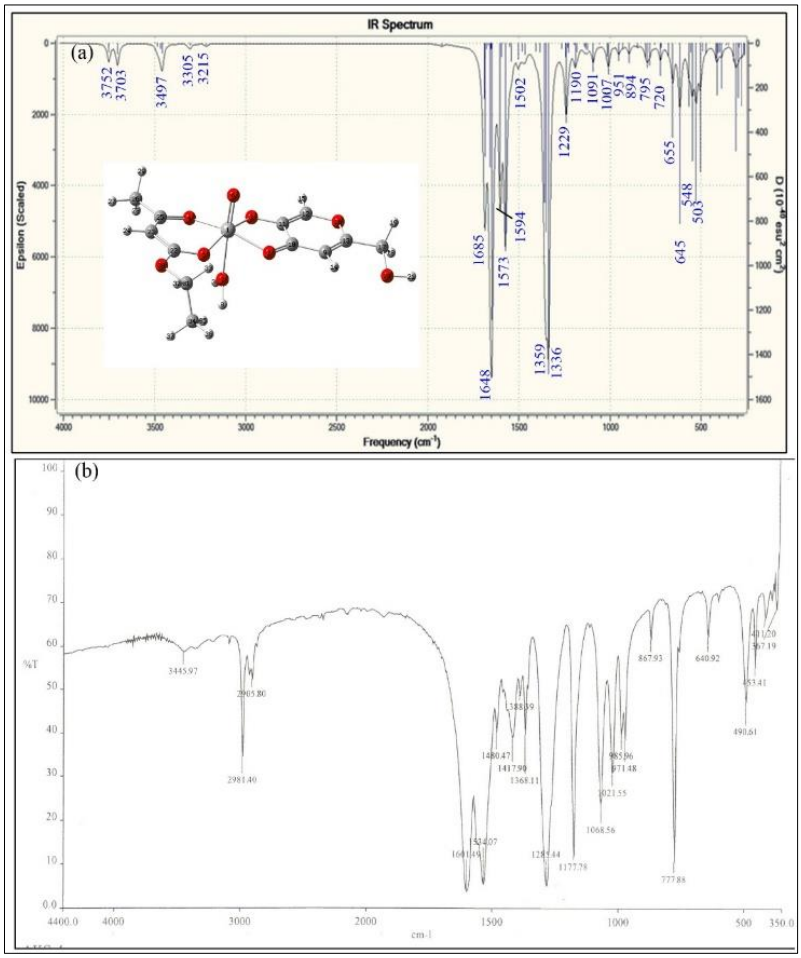

Figure 1. (a) Experimental; **(b)** theoretical FT-IR Spectrum of **C2**.

The electronic spectra of all the complexes were recorded in 10^{-3} M dimethylformamide, and their results are summarized in Table S1. Besides high-intensity charge transfer transitions, all these complexes {except compound **C2**} show **C2** to **C3** low-intensity d-d transitions, as shown in Figures S3 and S4.

The ESI-Mass spectrum of **C1** was recorded and presented in Figure S5. The spectral peaks observed in a compound at 149, 177, 199, 223,251, 279, 298, and 361 m/z are probably due to the two fragmentation routes shown in Scheme S1.

The X-band EPR spectrum of **C2** at liquid nitrogen temperature (LNT) was recorded on a powdered sample at 9.1 GHz, without using DPPH as a marker, as shown in Figure S6. The g factor is a dimensionless constant, and its actual value for a free electron is 2.0023. The shifting of the g value from 2.0023 towards the lower side suggests the mixing of the metal orbitals with the unpaired-electron orbitals in molecular orbitals. It can be said, in other words, that the metal-ligand bonds are covalent, and the compounds are paramagnetic [23].

3.2. Magnetic and conductance measurements.

The magnetically dilute VO(IV) complexes generally exhibit magnetic moments to their spin-only value of ~1.73 BM at room temperature. The magnetic moments observed for the studied complexes are in the range of 1.74 -1.79 B.M., which is typical for oxovanadium(IV) complexes that are magnetically dispersed. The magnetic moments are presented in the experimental section**.** These compounds had a molar conductance range of 19.7-23.4 ohm^{-1} cm^2 $mole^{-1}$ when tested in 10-3 M dimethylformamide solutions. The non-electrical nature of these complexes is evident in these values [24].

3.3. Powder XRD.

Figure 2a depicts the XRD pattern of the sample at room temperature. The XRD pattern shows the monoclinic crystal structure having a =5.0246, b =4.982, c =2.540. The lattice parameters of the selected unit cell were refined using the X'pert High Score Software (#JCPDS 00-050-1491), and all the peaks are indexed in Figure 2b. The average crystallite size and microstrain are calculated from the Williamson-Hall Relation [25].

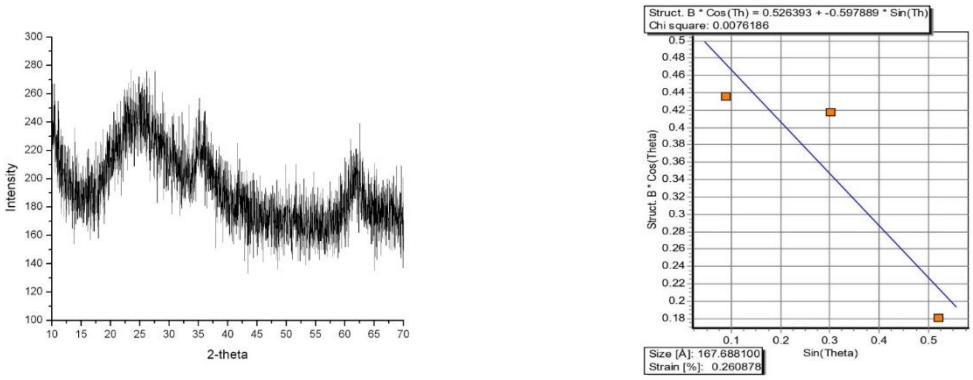

(a) **(b)**

Figure 2. (a) XRD Patterns of a complex **C2**; **(b)** Williamson-Hall plot of a complex **C2**.

$$\beta_{hkl}.\cos\theta = \frac{k\lambda}{D} + 4\varepsilon\sin\theta \qquad (2)$$

Where β_{hkl} represents the full width at half maximum intensity of individual peaks, λ is the wavelength of incident radiation, k represents a shape factor of about 0.94, D is crystallite size, and ε is the microstrain of the sample. The crystallite size is found to be 167Åor 16.7 nm

from the intercept, and the microstrain is about 0.2608% from the slope of the linear fit of the W-H plot, as shown in Figure 2b.

3.4. Electrochemistry.

Cyclic voltammetry has been used to study the electrochemistry of C2 and to monitor spectral and structural changes associated with electron-transfer reactions. The voltammogram was recorded in DMSO with tetrabutylammonium tetrafluoroborate, $[CH_3(CH_2)_3]_4NBF_4$ (TBATFB), as the supporting electrolyte over the potential range ±1000 mV versus current. Figure 3 depicts the voltammogram of **C2** and shows an irreversible redox wave. This may be due to a slow electron transfer reaction. The unusually high values of ΔE again fall within the range of 346.3-403.9 mV, not meeting the reversibility criterion [26]. The oxidations and reductions of the complex are achieved by the redox wave, which is the one-electron reduction at 403 mV, and the one-electron oxidation wave, which is the oxidation at -728 mV. The complex showed redox couples with a peak-to-peak separation (ΔEp) of 1131 mV, indicating a single-step one-electron transfer process.

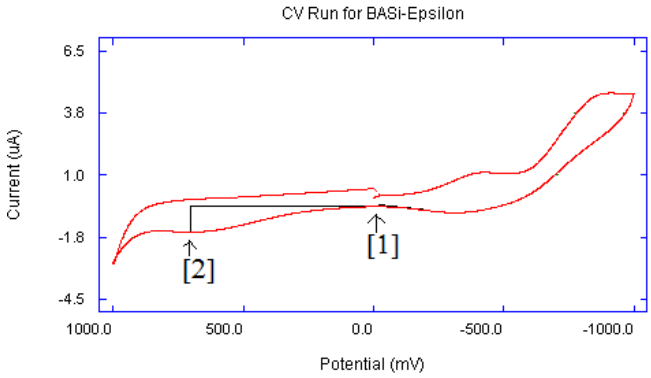

Figure 3. Cyclic voltammogram of **C2** in 0.20 M (TBATFB) [scan rate: 200 (mV/s)].

3.5. Theocratical chemistry.

3.5.1. DFT studies.

DFT is used to investigate the computed geometrical properties of C2, which are shown in Figure 4. The central vanadium ion is surrounded by six coordinates as V{O}6 environment. The first four coordination is associated with two monomeric bidentate mixed ligands like kojic acid and ethyl acetoacetate, which are in planar as V-O(2); 2.037 Å pyrone of kojic acid, V-O(3); 1.917 Å hydroxyl of kojic acid, V-O(4); 1.906 Å keto form, and V-O(5); 1.973 Å enolic form of ethyl acetoacetate. The fifth and sixth sites are equatorially coordinated by oxo oxygen, as V-O(6) (1.598 Å) and V-O(7) (2.177 Å), from the water molecule of the studied compound. The distorted octahedral geometry of **C2** is defined by the based on significant fifteen selected bond angles (°) along the vanadium center are: O(2)-V-O(3); 82.953, O(2)-V-O(4); 168.232, O(2)-V-O(5); 93.112, O(2)-V-O(6); 95.178, O(2)-V-O(7); 81.064, O(3)-V-O(4); 91.634, O(3)-V-O(5); 165.306, O(3)-V-O(6); 98.804, O(3)-V-O(7); 83.873, O(4)-V-O(5); 88.616, O(4)-V-O(6); 99.486, O(4)-V-O(7); 84.459, O(5)-V-O(6); 95.642, O(5)-V-O(7); 81.528 and O(6)-V-O(7); 172.209.

The frontier molecular orbitals (FMOs), especially the highest occupied molecular orbitals (HOMOs) and the lowest unoccupied molecular orbitals (LUMOs) have been widely used by chemists to understand the reactivity and regioselectivity of various chemical systems [27]. The energy difference between the HOMO and LUMO is termed the HOMO–LUMO gap

(ΔE) [28]. Although the HOMO–LUMO gap obtained from density functional calculations should be referred to as Kohn–Sham (KS) gap [29].

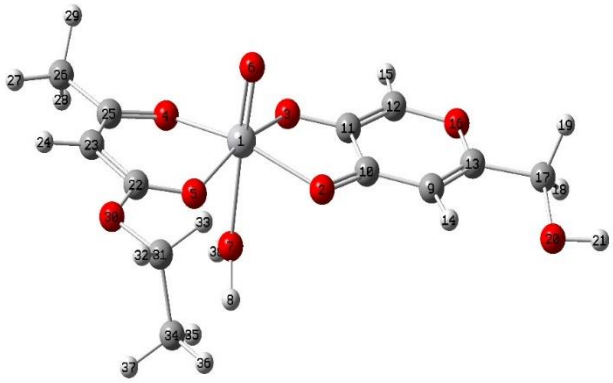

Figure 4. Optimized molecular structure of **C2** by B3LYP/LANL2MB basis set.

The sub-adjacent orbitals are labeled as NHOMO (the next-to-highest occupied molecular orbital) and SLUMO (the second-lowest unoccupied molecular orbital). These are also commonly referred to as HOMO-1 and LUMO+1, respectively. In the present investigation, we have selected six FMOs, namely, [HOMO-2] the third-highest, [HOMO-1] second highest, and [HOMO] highest occupied MO, the [LUMO], the lowest [LUMO+1] second-lowest, and [LUMO+2] third-lowest unoccupied MO's of kojic acid (H_2ka) and **C2** are shown in Figure S7 and Figure 5, respectively. The energies of the three HOMOs and three LUMOs of kojic acid in eV are HOMO-2; -7.509, HOMO-1; -6.557, HOMO; -6.375, LUMO; -1.219, LUMO-1; -0.2862, and LUMO-2; 1.283. The ΔE of HOMO-LUMO; 5.156, HOMO-1-LUMO+1; 6.271 and HOMO-2- LUMO+28.793 eV. Meanwhile, the FMOs of **C2** observed energies in the same order are -3.592, -3.176, -2.429, 0.541, 1.141, and 1.935 eV. The energy gap is also in the same order: 2.970, 4.455, and 5.526 eV. FMOs are one of the parameters that determine the magnetic properties of molecules. Kojic acid's diamagnetic properties are attributed to the presence of paired electrons in the HOMO. Although compound C2 is a paramagnetic compound, it does not have an unpaired electron in HOMO. Thus, the HOMO of C2 is regarded as a molecular orbital (SOMO) that has a single occupancy. The energy gap serves as an indicator of the compound's kinetic stability and chemical reactivity [30,31]. This abbreviation may also be extended to semi-occupied molecular orbital. Koopmans's theorem [32,33] is used to calculate the energies of the frontier orbitals of molecules, including their ionization energy and electron affinity.

$$-E_{HOMO} = IE \quad (3)$$

$$-E_{LUMO} = EA \quad (4)$$

The absolute electronegativity (χ_{abs}) and absolute hardness (η) are associated with IA and EA [34] as given below:

$$\chi_{abs} = (IE + EA)/2 = (E_{HOMO} + E_{LUMO}) / 2 \quad 5)$$

$$\eta = (IE - EA)/2 = (E_{HOMO} - E_{LUMO}) / 2 \quad (6)$$

The energy gap (ΔE) defines the softness and hardness of a molecule. If a molecule has a large energy gap, it is hard; soft molecules have a small energy gap [34]. The absolute electronegativity (χ_{abs}), absolute hardness (η) of kojic acid, and **C2** are calculated using equations (3) to (6) and are represented in Table S2. There is a much smaller energy gap in the complex than in the ligands. Another important property related to the dipole moment and hardness is the electrophilicity index (ω), and global softness (S) is calculated by given equations (7) and (8). The values of ω and S are given in Table S2.

$$\omega = \mu^2 / 2\eta \quad (7)$$

$$S = 1/\eta \quad (8)$$

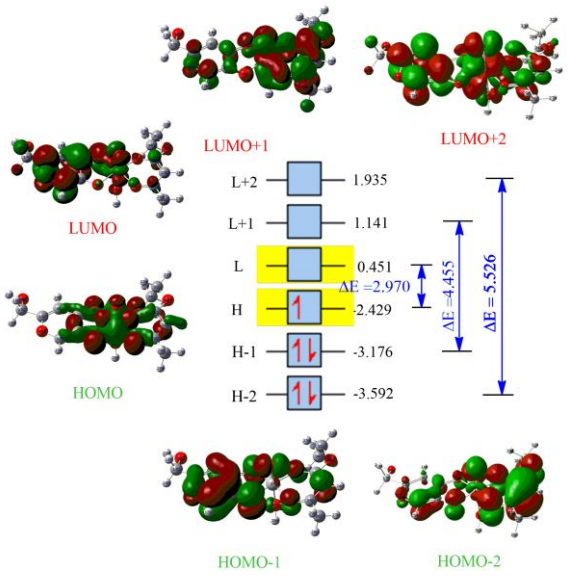

Figure 5. FMO's structure with energy level diagram of **C2** values is given in eV.

In chemistry, the charge of an atom is a fundamental and classical concept. DFT is used to perform the charge analysis, which is a crucial parameter for molecules. Mulliken's atomic charge [35] is defined in terms of orbitals. All electronic charge contributions from orbitals centered at that atom are summed up for each atom, and electronic overlap clouds between two atoms are distributed evenly between them. Here, we investigated charge analysis of **C2** by two reliable and well-known methods: (i) Natural population analysis (NPA) and (ii) Mulliken analysis with a B3LYP/LANL2MB basis set. Comparing the analyses is difficult due to the diverse theoretical backgrounds of the methods. Upon reviewing the results, I noticed surprising differences between Mulliken's and NPA charges. According to the results, NPA and Mulliken analyses indicate that all hydrogens and carbons, such as C10, C11, C13, C22, C25, and V1, have a positive charge. All oxygens O2, O3, O4, O5, O6, O7, O16, O20, and O30, as well as the remaining atoms, C9, C23, C24-C26, and all oxygens O2, O3, O4, O5, O6, O7, O16, O20, and O30, exhibit a negative charge. Positive charges are present in Mulliken analysis for the atoms named C12, C17, and C31, while negative charges are present in NPA. Figure S8 depicts the presentation of these in a graph. The color scale of positive and negative charges for (a) Mulliken atomic charges and (b) NPA atomic charges is shown in Figure S9, and data are charted in Table S3.

The MESP is an acronym for the molecular electrostatic potential surface; it is used to understand the reactive behavior of a molecule in its negative and positive regions, which can be regarded as nucleophilic and electrophilic sites, respectively. The molecular electrostatic potential surface is used to record the molecular shape, size, and electrostatic potential values of kojic acid and C2. The MESP diagram of kojic acid shows that the carbonyl oxygen and hydroxyl oxygen atoms represent the large negative potential regions, while in the case of **C2**, the coordination environment with {O6} and vanadium (central atom) is the region of most negative potential. The hydrogen atoms in kojic acid bear the region of maximum positive charge, while the regions of maximum positive charge are the hydrogens of the two ligands, kojic acid, and ethyl acetoacetate, in the case of **C2**, as shown in Figure S10. The coordinated

water molecule has two most electropositive hydrogens attached to its electronegative oxygen, which is noteworthy. A potential halfway point between red and dark blue is where the predominant green region in the MESP surfaces lies.

3.5.2. Molecular docking evaluation.

All the ligands were docked on the crystal structure of human CYP3A4 bound to metformin. The co-crystallized metformin (MF8) creates one hydrogen bond with ARG 212 (2.937 Å). The docking pose of the co-crystallized metformin (MF8) interacting with amino acid residues of the active site is shown in Figure 6 and Table 1. Kojic acid was used as a reference ligand to compare the docking results of all the studied compounds. Kojic acid showed the occurrence of four hydrogen bonds, two with the same amino acid, co-crystallized MF8, ARG 212 (2.886 Å; 2,926 Å), and two with ARG 105 (2.806 Å; 2.972 Å). These are shown in Figure 7. The docking score of all ligands is greater than the docking score of the co-crystallized and the docking score of Kojic acid. The docking studies have shown that **C1** forms seven hydrogen bonds: four with the same amino acid as co-crystallized MF8, ARG 212 (2.986 Å; 3.063 Å; 3.171 Å; 3.236 Å), and ARG 106 (3.043 Å), and two with GLU 374 (3.238 Å; 2.916 Å). The **C2** (docking score: -44.22; RMSD: 0.11 Å) shows the occurrence of seven hydrogen bonds, three with the same amino acid as co-crystallized MF8, ARG 212 (3.108 Å; 2.941 Å, 2.862 Å), with ARG 105 (3.105 Å), SER 119 (2.807 Å), ARG 372 (3.144 Å) and with ALA 370 (2.609 Å). Also, **C3** (docking score: -43.41; RMSD: 0.03 Å) forms six hydrogen bonds, five with the same amino acid as co-crystallized MF8, ARG 212 (3.150 Å, 2.893 Å, 3.164 Å, 3.074 Å, 3.186 Å) and with SER 119 (3.109 Å), and two with GLU 374 (3.238 Å, 2.916 Å). **C4** has been predicted to have a significant docking score (-53.52, RMSD: 0.05); this compound forms four hydrogen bonds with ARG 212 (3.048 Å), ARG 372 (3.008Å), ALA 370 (3.056 Å), and ILE 369 (2.847 Å). The docking pose of the co-crystallized ligand and its interaction with the amino acid residues of the active site of 5Q5J are shown in Figure 8. The amino acid residues forming the interacting groups for each ligand are listed in Table 2. The docking score decreases in order: C**4** (docking score-53.52, RMSD: 0.05)> C**2** (docking score: -44.22; RMSD: 0.11 Å)> **C3** (docking score: -43.41; RMSD: 0.03 Å)>**C1** (docking score: -40.02; RMSD: 0.03 Å)>Kojic acid (docking score -35.44, RMSD: 0.03)>co-crystallized (docking score: -28.21; RMSD: 0.11 Å). It is presented in Figure 9.

Table 1. The list of intermolecular interactions between the compounds docked with 5G5J.

Ligand	Score*	RMSD Å	Group interaction	Hydrogen bond**	Bond length Å
Co-crystallized MF8	-28.21	0.11	ARG 105, SR 119, ILE 301, PHE 304, ARG 212, ALA 305, ALA 370, ARG 372, LEU 373	N sp^3 (ON06)- N sp^2 -ARG 212	2.937
Kojic acid	-35.44	0.03	ARG 105, GLU 374, SER 119, ARG 375, ARG 372, ALA 370, LEU 373, ALA 305, ARG 212.	O sp^3 (O1)-N sp^2-ARG 212 O sp^2 (O2)-N sp^3- ARG 212 O sp^2 (O3)-N sp^2 - ARG 105 O sp^3 (O4)-N sp^2 - ARG 105	2.886 2.926 2.806 2,972
1	-40.02	0.03	ARG 105, PHE 108, ASP 76, PRO 107, ARG 106, GLU 374, SER 119, ARG 375, ARG 372, ALA 370, PHE 215, LEU 373, PHE 213, ALA 305, ARG 212, PHE 304, ILE 301.	O sp^2 (O2)-N sp^2 - ARG 212 O sp^2 (O2)-N sp^2 - ARG 212 O sp^3 (O20)-N sp^2 - ARG 212 O sp^3 (O7)-N sp^2 - ARG 212 O sp^3 (O17)-O sp^2 - GLU 374 O sp^3 (O17)- N sp^2 -ARG 106 O sp^3 (O17)-O sp^3- GLU 374	2.986 3.063 3.171 3.236 3.238 3.043 2.916

Ligand	Score*	RMSD Å	Group interaction	Hydrogen bond**	Bond length Å
2	-44.22	0.11	ARG 105, PHE 108, ARG 106, ILE 420, GLU 374, SER 119, ARG 372, ALA 370, MET 371, PHE 57, GLY 481, PHE 215, LEU 482, LEU 373, PHE 213, ALA 305, ARG 212, PHE 304, ILE 301.	O sp^2 (O2)-N sp^2 - ARG 105 O sp^3 (O20)-N sp^2 - ARG 212 O sp^3 (O12)-N sp^2 - ARG 212 O sp^3 (O11)-N sp^2 - ARG 212 O sp^3 (O7)- O sp^3 – SER 119 O sp^3 (O17)-N sp^2- ARG 372 O sp^3 (O17)-O sp^3- ALA 370	3.155 3.108 2.941 2.862 2.807 3.144 2.609
3	43.41	0.03	ARG 105, ARG 106, GLU 374, SER 119, ARG 372, ALA 370, MET 371, ILE 369, PHE 57, GLY 481, PHE 215, GLY 81, LEU 482, LEU 483, PHE 213, ALA 305, ARG 212, THR 309, PHE 304, PHE 302, ILE 301, ILE 118.	O sp^2 (O18)-N sp^2 - ARG 212 O sp^2 (O18)-N sp^2 - ARG 212 O sp^2 (O11)-N sp^2 - ARG 212 O sp^2 (O11)-N sp^2 - ARG 212 O sp^3 (O21)- N sp^2 - ARG 212 O sp^3 (O26)-O sp^3-SER 119	3.150 2.893 3.164 3.074 3.186 3.109
4	-53.52	0.05	ARG 105, ARG 106, GLU 374, PRO 107, ILE 120, SER 119, PHE 108, LEU 373, ARG 372, ALA 370, MET 371, ILE 369, PHE 57, PHE 215, GLY 81, LEU 482, LEU 483, PHE 213, ARG 212, THR 309, PHE 304.	O sp^3 (O1)-O sp^2 - ARG 372 O sp^3 (O1)-O sp^2 – ALA 370 O sp^3 (O21)- O sp^2 – ILE 369 O sp^2 (O20)-N sp^2- ARG 212	3.008 3,056 2.847 3.048

*The docking score ($PLANTS_{PLP}$ score) is a function described in [36]. ** The numbering of the atoms was done according to the software (Figure 11).

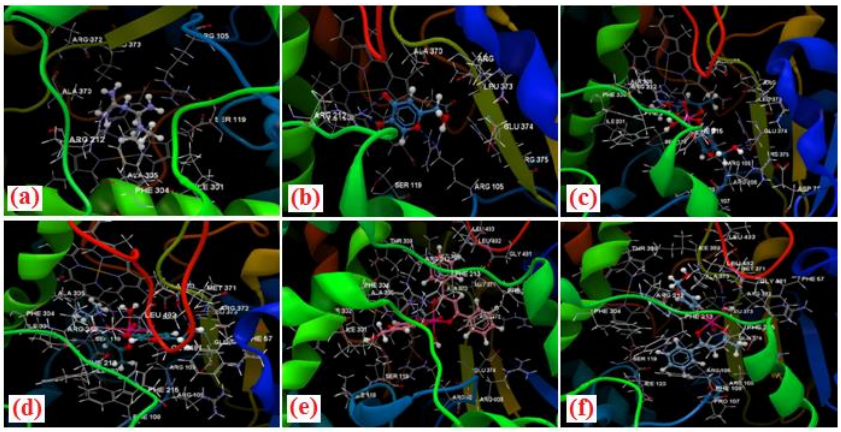

Figure 6. Docking pose of the **(a)** co-crystallized metformin (MF8); (b) kojic acid; **(c)** C1; **(d)** C2; **(e)** C3; **(f)** C4, interacting with amino acid residues of the active site.

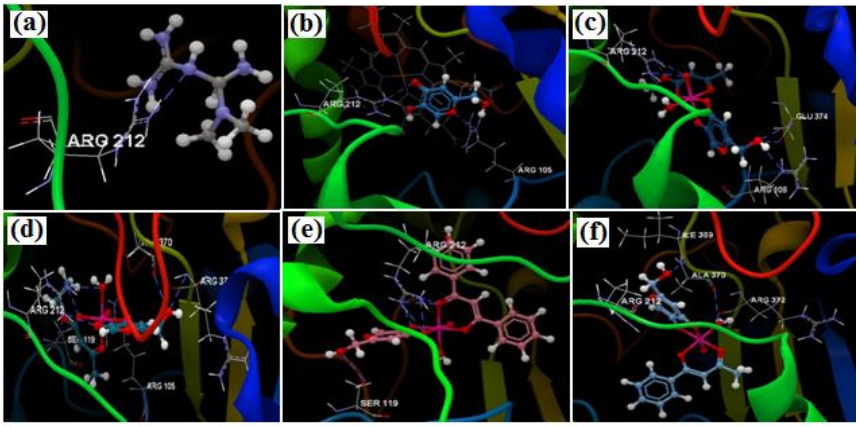

Figure 7. Hydrogen bond (blue dotted lines) between **(a)** co-crystallized metformin MF8 and ARG 212 amino acid; **(b)** kojic acid and ARG 212 and ARG 105 amino acids; **(c) C1** and ARG 212, ARG 106 and GLU 374 amino acids; **(d) C2** and ARG 212, ARG 105, ARG 372, SER 119 and ALA 370 amino acids; **(e) C3** and ARG 212 and SER 119 amino acids; **(f) C4** and ARG 212, ARG 372, ILE 359 and ALA 370 amino acids.

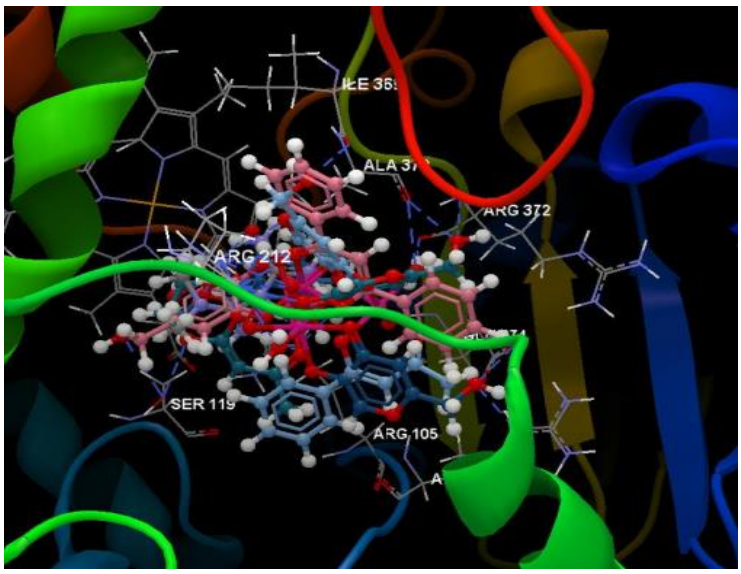

Figure 8. Docking pose of the co-crystallized MF8 of the studied compounds in the binding site of 5Q5J.

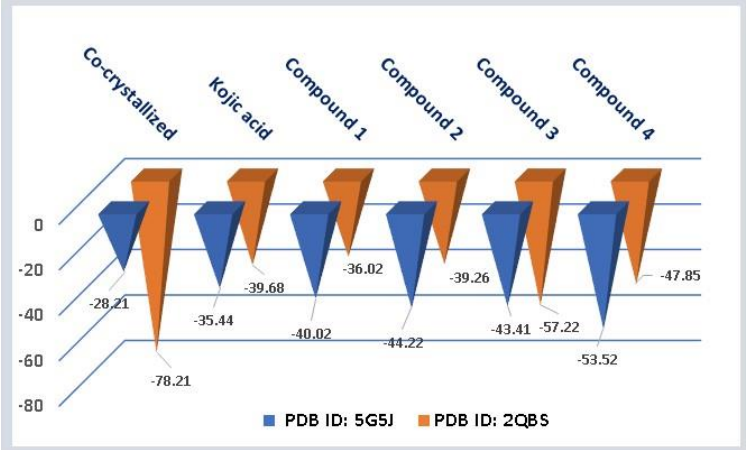

Figure 9. Docking scores of all the molecules.

Docking evaluation on ptp1b-inhibitor complex (PDB ID: 2QBS): Kojic and all the synthesized complex compounds were also docked on the crystal structure of the Protein Tyrosine Phosphatase complex (PTP-C). The co-crystallized 4-bromo-3-(carboxymethoxy)-5-[3-(cyclohexylamino)phenyl]thiophene-2-carboxylic acid (024) created seven hydrogen bonds with TYR 46 (3.078 Å), LYS 120 (3.125 Å), GLN 266 (2.897 Å), PHE 182 (2.746 Å), and two hydrogen bonds with ARG 221(3.060 Å, 3.052 Å). The docking pose of the co-crystallized (024) interacting with amino acid residues of the active site is shown in Figure 10. Kojic acid was used as a reference ligand to compare the docking results of all studied compounds. Kojic acid shows the occurrence of five hydrogen bonds with TYR 46 (3.074 Å), LYS 120 (3.107 Å), ARG 221(3.124 Å), PHE 182 (3.095 Å), and GLN 266 (2.911 Å) (Figure 10). The docking studies revealed that C1 formed two hydrogen bonds with TYR 46 (3.075 Å) and with LYS 120 (2.904 Å) (Figure S11). Compound 2 shows the occurrence of four hydrogen bonds, two with ARG 47 (2.750 Å; 3.322 Å) and two with ASP 48 (3.085 Å, 2.925 Å) (Figure S11). The C3 has been predicted to have a significant docking score (-57.22, RMSD: 0.20); this compound forms three hydrogen bonds with ASP 48 (3.187 Å) and two GLN 262 (2.978 Å, 2.933 Å). It was observed that C4 does not form hydrogen bonds with the amino acid residues in the protein receptor's active site.

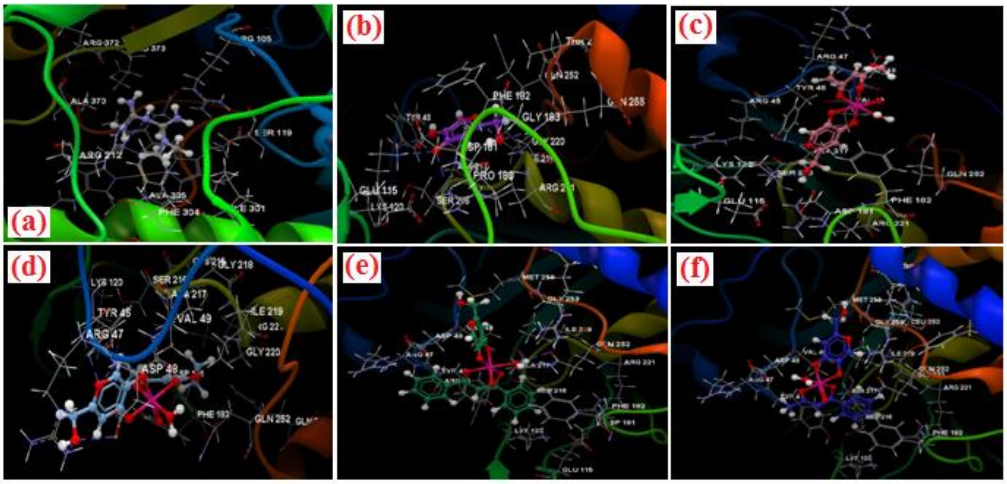

Figure 10. Docking pose of the **(a)** co-crystallized (024); **(b)** kojic acid and complexes; **(c)** C1; **(d)** C2; **(e)** C3; **(f)** C4 interacting with amino acid residues of the active site.

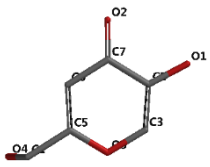

Kojic Acid

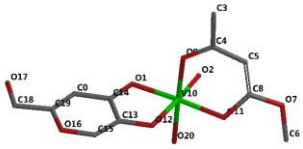

C1

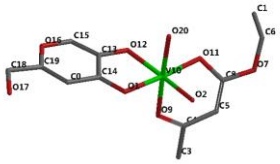

C2

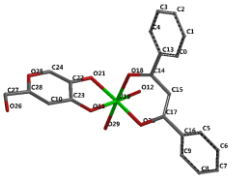

C3

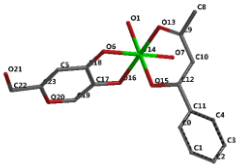

C4

Figure 11. Tube representation of the optimized molecular structure of studied compounds kojic acid and **C1-C4** (the numbering of the atoms was done according to the Spartan software).

The docking pose of the co-crystallized and the ligands interacting with amino acid residues of the active site of 5Q5J are shown in Figure S12. The amino acid residues forming the interacting groups for each ligand are listed in Table S5. The docking score decreases in order: co-crystallized (docking score: -78.21; RMSD: 0.42Å)>C**3** (docking score: -57.22; RMSD: 0.20Å) > **C4** (docking score-47.85, RMSD: 0.06) > Kojic acid (docking score -39.68; RMSD: 0.01) > compound **2** (docking score: -39.26; RMSD: 0.53Å) >**C1** (docking score: -36.02; RMSD: 0.01Å) Table S5. The docking studies revealed that the docking scores of all the ligands are lower than that of the co-crystallized ligand (024), and only 2 complex compounds, C3 and C4, have higher docking scores than kojic acid (Figure 7).

After analyzing the data from the docking study, it was observed that all the studied compounds were placed in the same binding site of the protein receptor (PDB ID: 2QBS) as the co-crystallized ligand and kojic acid. Only C1 showed the occurrence of two hydrogen bonds with the same amino acids TYR 46 and LYS 120 as the co-crystallized, 4-bromo-3-

(carboxymethoxy)-5-[3-(cyclohexylamino)phenyl]thiophene-2-carboxylic acid (024) and the kojic acid Figure S11. The number of violations of the Lipinski rules allows drug-likeness evaluation for a molecule. All the studied compounds were observed to respect Lipinski's rule of five. According to Lipinski's rule, the calculated parameters are the number of hydrogen donors < 5, the number of hydrogen acceptors < 10), molecular weight < 500 Da, and the octanol-water partition coefficient (log *P*) < 5 (Table 2).

Table 2. Calculated properties of compounds.

Compounds	Atoms	Weight (Daltons)	Flexible bonds	Lipinski violations	Hydrogen donors	Hydrogen acceptors	Log P
Co-crystallized*	24	133.20	3	1	8	5	1.15
Co-crystallized**	45	452.32	7	1	1	6	6.84
Kojic acid	16	142.11	1	0	2	4	0.59
C1	35	341.16	2	0	3	9	1.84
C2	38	355.19	3	0	3	9	2.21
C3	48	449.30	3	0	3	8	4.56
C4	41	387.23	4	0	3	8	3.30

* PDB ID: 5G5J; ** PDB ID: 2QBS.3.5.3. Insilco ADME studies.

The online server was used to obtain the *in silico* ADME properties. Details are provided in the experimental section. This method uses Classical physicochemical properties to predict absorption, distribution, metabolism, excretion, and toxicity (ADMET). The biological potential and oral administrative activities of these studies are showing good results. The Swiss ADME predictor gives more data on drugs, including molecular hydrophobicity (log P), topological polar surface area (TPSA), and bioavailability. Five CYP models (i) CYP1A2, (ii) CYP2C19, (iii) CYP2C9, (iv) CYP2D6, and (v) CYP3A4 inhibitors, along with one phosphatase glycoprotein (P-GP) substrate, are used to predict the metabolism. These parameters were computed and confirmed in agreement with their standard ranges. The *in silico* ADME properties of all the complexes are charted in Table S6. Figure S13 depicts the Egg model of cheminformatics and the physicochemical properties of C1-**C4**. The topological polar surface area is a highly applicable physicochemical parameter, analyzed using hydrogen-bonding metrics, and is useful for predicting drug transport properties across various body compartments, including the gastrointestinal tract and blood-brain barrier penetration. The compound contains several hydrogen bond donors (HBD) and some hydrogen bond acceptors (HBA). The compound's composition includes nine rotatable bonds, indicating that it is intended for oral administration. Observations of our compounds that meet only the two criteria of first rotatable bonds (10 or fewer) and second polar surface area equal to or less than 140 Å2 (or 12 or fewer H-bond donors and acceptors) will have a high probability of good oral bioavailability in the rat. Moreover, the bioactive score is greater than zero, indicating a higher probability, and the biological activity of the examined compound increases. Lipophilicity, as measured here by computed logP values, plays a vital role in determining ADME parameters and the molecule's potency. According to Lipinski's rule, the log P values are less than 5, indicating a greater tendency to facilitate penetration of the cell membrane. The log P values of the studied compounds were less than 5, indicating a greater tendency to penetrate the cell membrane. The solubility score (logS) explains the solubility of the molecules. It is defined in the given scale < 0; highly soluble, < -2; soluble, < -4; moderately soluble < -6; poorly soluble, and < -10; insoluble. The log S values for the studied complexes C1 and C2 are below -2.00, indicating low solubility in water, while the complexes C3 and C4 have moderate solubility in water because their log S values are above -2.00.

3.6. Antibacterial studies.

The biological activity of the kojic acid and oxovanadium(IV) complexes **C1-C4** were tested against (Gram-positive bacteria *Lactobacillus* and *E. Cocus*) and (Gram-negative bacteria *E. coli* and S. Typhi) using Ampicillin as a standard antibacterial drug. The diffusion agar technique [37] (of 300 μg cm^{-3} in DMSO) was used to evaluate the activity. The results of bactericidal screening of the synthesized compounds are recorded in Table 3, and a graphical representation is shown in Figure S14. Antibacterial activity of the metal complexes is found to be greater than the ligand and depends upon the metal ions, i.e., size, charge distribution, shape, and redox potential of the metal chelates and chelation [38]. Certainly, steric and pharmacokinetic factors also play a decisive role in deciding the potency of an antimicrobial agent. Metal complexes possess an antibacterial property, a complex blend of multiple contributions.

Table 3. Antibacterial activity of kojic acid and two representative complexes in mm.

Compounds	Gram-positive bacteria		Gram negative bacteria	
	Lactobacillus	*E. Cocus*	*S. Typhi*	*E-Coli*
Kojic acid	5	-	10	-
[VO(ka)(macac)(H_2O)] C1	22	-	11	14
[VO(ka)(dbm)(H_2O)] C3	-	12	10	12
Ampicillin	>10	>10	>10	>10

4. Conclusions

In this manuscript, we synthesized the VO(IV) complexes of monomeric bidentate mixed-ligands: kojic acid and substituted β-ketoenolates. These complexes were formulated as [VO(ka)(L)(H_2O)] where ka = kojic acid and LH= β-ketonolates. Physiochemical and spectroscopic techniques have characterized these complexes. Theoretical chemistry was performed using DFT calculations, molecular docking, and an *in silico* ADME approach. The molecular structure, vibrational wavenumbers, and infrared intensities were obtained for the molecule using the B3LYP density functional theory (DFT) with the standard B3LYP/6-31+G(d, p)/LANL2DZ basis set. Theoretical calculations, primarily geometry optimization, charge distributions, and FMOs, were performed using density functional theory. The experimental results and the calculated molecular parameters, including interatomic distances and angles, revealed a distorted octahedral geometry for the compound. Moreover, the *in silico* ADME parameter, log P was observed to be less than 5 (**C1**; -1.79, **C2**; -1.51, **C3**; 0.23, and **C4** -0.63**),** representing a higher tendency to penetrate the cell membrane. The solubility score (logS) of **C1** and **C2** is less than -2.00, representing the solubility in water, while **C3** and **C4** are moderately soluble in water because the log S values are more than -2.00.

Author Contributions

Writing – review & editing, P. K. V., R. C. M., P. S. J., A. K. S., S. R., R. K. M., and L. P. All authors have read and agreed to the published version of the manuscript.

Institutional Review Board Statement

Not applicable.

Informed Consent Statement

Not applicable.

Data Availability Statement

Data supporting the findings of this study are available upon reasonable request from the corresponding author.

Funding

This project does not have support.

Acknowledgments

We are grateful to the Bioscience Department of Rani Durgavati Vishwavidyalaya, Jabalpur; the Central Drug Research Institute, Lucknow; the Regional Sophisticated Instrumentation Centre, Indian Institute of Technology, Mumbai; and the Roorkee for providing analytical facilities. The authors are also thankful to Prof. Rajesh Kumar Verma, Rani Durgavati Vishwavidyalaya, Jabalpur, and Principal, Govt. Digvijay Autonomous PG College, Rajnandgaon (CG), for motivation and encouragement.

Conflicts of Interest

The author declares no conflicts of interest.

References

1. Zborowski, K.; Proniewicz, L.M. Aromaticity properties of kojic acid and maltol complexes with oxovanadium (IV) ion. *Pol. J. Chem.* **2004**, *78*, 2219-2223.
2. Burdock, G.A.; Soni, M.G.; Carabin, I.G. Evaluation of Health Aspects of Kojic Acid in Food. *Regul. Toxicol. Pharmacol.* **2001**, *33*, 80-101, https://doi.org/10.1006/rtph.2000.1442.
3. Zborowski, K.; Grybos, R.; Proniewicz, L.M. Determination of the most stable structures of selected hydroxypyrones and their cations and anions. *J. Mol. Struct. THEOCHEM* **2003**, *639*, 87-100, https://doi.org/10.1016/S0166-1280(03)00586-4.
4. Ismael, M.; Abdel-Mawgoud, A.-M.M.; Rabia, M.K.; Abdou, A. Design and synthesis of three Fe(III) mixed-ligand complexes: Exploration of their biological and phenoxazinone synthase-like activities. *Inorganica Chim. Acta* **2020**, *505*, 119443, https://doi.org/10.1016/j.ica.2020.119443.
5. Abdel-Rahman, L.H.; El-Khatib, R.M.; Nassr, L.A.E.; Abu-Dief, A.M. Synthesis, physicochemical studies, embryos toxicity and DNA interaction of some new Iron(II) Schiff base amino acid complexes. *J. Mol. Struct.* **2013**, *1040*, 9-18, http://dx.doi.org/10.1016/j.molstruc.2013.02.023.
6. Abdel-Rahman, L.H.; Basha, M.T.; Al-Farhan, B.S.; Alharbi, W.; Shehata, M.R.; Al Zamil, N.O.; Abou El-ezz, D. Synthesis, Characterization, DFT Studies of Novel Cu(II), Zn(II), VO(II), Cr(III), and La(III) Chloro-Substituted Schiff Base Complexes: Aspects of Its Antimicrobial, Antioxidant, Anti-Inflammatory, and Photodegradation of Methylene Blue. *Molecules* **2023**, *28*, 4777, https://doi.org/10.3390/molecules28124777.
7. Nariya, P.; Thakore; S. Synthesis, characterization, DFT calculations and application of some metal complexes derived from 2-(((2-(dimethylamino)ethyl)amino)(4-nitrophenyl)methyl)-3-hydroxynaphthalene-1,4-dione. *Inorg. Chem. Commun.* **2023**, *151*, 110651, https://doi.org/10.1016/j.inoche.2023.110651.
8. Sharma, B.P.; Subin, J.A.; Marasini, B.P.; Adhikari, R.; Pandey, S.K.; Sharma, M.L. Triazole based Schiff bases and their oxovanadium(IV) complexes: Synthesis, characterization, antibacterial assay, and computational assessments. *Heliyon* **2023**, *9*, e15239, https://doi.org/10.1016/j.heliyon.2023.e15239.

9. Ghorbani, P.; Ali, B.S.; Homayouni-Tabrizi, M.; Yaghmaei, P. Oxovanadium(IV) complexes of the pyridoxal Schiff bases: synthesis, experimental and theoretical characterizations, QTAIM analysis and antioxidant activity. *J. Serb. Chem. Soc*. **2020**, *85*, 37–51, https://doi.org/10.2298/JSC190129055G.
10. Frisch, M. J.; Trucks, G.W.; Schlegel, H.B.; Scuseria, G.E.; Robb, M.A.; Cheeseman, J.R.; Zakrzewski, V.G.; Montgomery, Jr, J.A.; Stratmann, R.E;, Burant, J.C.; Dapprich, S., Millam, J.M.; Daniels, A.D.; Kudin, K.N;, Strain, M.C.; Farkas, O.; Tomasi, J.; Barone, V.; Cossi, M.; Cammi, R.; Mennucci, B.; Pomelli, C.; Adamo, C.; Clifford, S.; Ochterski, J.; Petersson, G.A.; Ayala, P.Y.; Cui, Q.; Morokuma, K.; Reg, N.; Salvador, P.; Dannenberg, J.J.; Malick, D.K.; Rabuck, A.D.; Rahavachari, K.; Foresman, J.B.; Cioslowski, J.; Ortiz, J.V.; Baboul, A.G.; Stefanov, B.B.; Liu, G.; Liashenko, A.; Komaromi, P.P.; Gomperts, R.; Martin, R.L.; Fox, D.; Keith, T.; AlLaham, M.A.; Peng, C.Y.; Nanayakkara, A.; Challa Combe, M.; Gill, P.; Johnsom, B.; Chen, W.; Wong, M.W.; Andres, J.L.; Gonzalez, Head Gordon, M.; Replogle, E.S.; Pople, J.A. Gaussian09, Revision A11.4, Gaussian Inc Pittsburgh **2010**.
11. Gauss View 9.0, Gaussian Inc., Garnegie office. Park. Pittsburgh. PA, USA.
12. Basaleh, A.S.; Alomari, F.Y.; Sharfalddin, A.A.; Al-Radadi, N.S.; Domyati, D.; Hussien, M.A. Theoretical Investigation by DFT and Molecular Docking of Synthesized Oxidovanadium(IV)-Based Imidazole Drug Complexes as Promising Anticancer Agents. *Molecules* **2022**, *27*, 2796, https://doi.org/10.3390/molecules27092796.
13. Singh, J.S.; Khan, M.S.; Uddin, S. A DFT study of vibrational spectra of 5-chlorouracil with molecular structure, HOMO–LUMO, MEPs/ESPs and thermodynamic properties. *Polym. Bull.* **2023**, *80*, 3055-3083. https://doi.org/10.1007/s00289-022-04181-7.
14. Agu, P.C.; Afiukwa, C.A.; Orji, O.U.; Ezeh, E.M.; Ofoke, I.H.; Ogbu, C.O.; Ugwuja, E.I.; Aja, P.M. Molecular docking as a tool for the discovery of molecular targets of nutraceuticals in diseases management. *Sci. Rep.* **2023**, *13*, 13398, https://doi.org/10.1038/s41598-023-40160-2.
15. Guo, Z.; Sevrioukova, I.F.; Denisov, I.G.; Zhang, X.; Chiu, T.-L.; Thomas, D.G.; Hanse, E.A.; Cuellar, R.A.D.; Grinkova, Y.V.; Langenfeld, V.W. Heme Binding Biguanides Target Cytochrome P450-Dependent Cancer Cell Mitochondria. *Cell Chem. Biol.* **2017**, *24*, 1259-1275, http://dx.doi.org/10.1016/j.chembiol.2017.08.009.
16. Wilson, D.P.; Wan, Z.-K.; Xu, W.-X.; Kirincich, S.J.; Follows, B.C.; Joseph-McCarthy, D.; Foreman, K.; Moretto, A.; Wu, J.; Zhu, M.; Binnun, E.; Zhang, Y.-L.; Tam, M.; Erbe, D.V.; Tobin, J.; Xu, X.; Leung, L.; Shilling, A.; Tam, S.Y.; Mansour, T.S.; Lee, J. Structure-Based Optimization of Protein Tyrosine Phosphatase 1B Inhibitors: From the Active Site to the Second Phosphotyrosine Binding Site. *J. Med. Chem.* **2007**, *50*, 4681-4698, https://doi.org/10.1021/jm0702478.
17. Sarangi, A.K.; Mahapatra, B.B.; Mohapatra, R.K.; Sethy, S.K.; Das, D.; Pintilie, L.; Kudrat-E-Zahan, M.; Azam, M.; Meher, H. Synthesis and characterization of some binuclear metal complexes with a pentadentate azodye ligand: An experimental and theoretical study. *Appl. Organomet. Chem.* **2020**, *34*, e5693, https://doi.org/10.1002/aoc.5693.
18. Mohapatra, R.K.; Perekhoda, L.; Azam, M.; Suleiman, M.; Sarangi, A.K.; Semenets, A.; Pintilie, L.; Al-Resayes, S.I. Computational investigations of three main drugs and their comparison with synthesized compounds as potent inhibitors of SARS-CoV-2 main protease (M^{pro}): DFT, QSAR, molecular docking, and in silico toxicity analysis. *J. King Saud Univ. Sci.* **2021**, *33*, 101315, https://doi.org/10.1016%2Fj.jksus.2020.101315.
19. Ononamadu, C.J.; Ibrahim, A. Molecular docking and prediction of ADME/drug-likeness properties of potentially active antidiabetic compounds isolated from aqueous-methanol extracts of Gymnema sylvestre and Combretum micranthum. *BioTechnologia* **2021**, *102*, 85-99, https://doi.org/10.5114/bta.2021.103765.
20. Selbin, J. Oxovanadium(IV) complexes. *Coord. Chem. Rev.* **1966**, *1*, 293-314, https://doi.org/10.1016/S0010-8545(00)80142-3.
21. Maurya, R.C.; Singh, H.; Pandey, A.; Singh, T. Metal chelates of bioinorganic and catalytic relevance: Synthesis, magnetic and spectral studies of some mononuclear and binuclear oxovanadium(IV) and dioxotungsten(VI) complexes involving Schiff bases derived from 4-butyryl-3- methyl-1-phenyl-2-pyrazolin-5-one and certain aromatic amine. *Indian J. Chem.* **2001**, *40A*, 1053-1063.
22. Maurya, R.C.; Rajput, S. Oxovanadium(IV) complexes of bioinorganic and medicinal relevance: synthesis, characterization, and 3D molecular modeling and analysis of some oxovanadium(IV) complexes involving O,O-donor environment. *J. Mol. Struct.* **2004**, *687*, 35-44, https://doi.org/10.1016/j.molstruc.2003.08.023.
23. Dutta, R.L.; Syamal, A. Elements of Magneto Chemistry, 2nd Edition, Affiliated East West Press, New Delhi, **1993**.

24. Geary, W.J. The use of conductivity measurements in organic solvents for the characterisation of coordination compounds. *Coord. Chem. Rev.* **1971**, *7*, 81-122, https://doi.org/10.1016/S0010-8545(00)80009-0.
25. Nath, D.; Singh, F.; Das, R. X-ray diffraction analysis by Williamson-Hall, Halder-Wagner and size-strain plot methods of CdSe nanoparticles - a comparative study. *Mater. Chem. Phys.* **2020**, *239*, 122021, https://doi.org/10.1016/j.matchemphys.2019.122021.
26. Kissinger, P.T.; Heineman, W.R. Laboratory Techniques in Electroanalytical Chemistry, 2nd Edition, Revised and Expanded. Kissinger, P.T. Heineman W.R., Eds.; Marcel Dekker: New York, **1996**, https://doi.org/10.1201/9781315274263.
27. Yu, J.; Su, N.Q.; Yang, W. Describing Chemical Reactivity with Frontier Molecular Orbitalets. *JACS Au* **2022**, *2*, 1383–1394, https://doi.org/10.1021/jacsau.2c00085.
28. Parte, M.K.; Vishwakarma, P.K.; Jaget, P.S.; Maurya, R.C. Synthesis, spectral, FMOs and NLO properties based on DFT calculations of dioxidomolybdenum(VI) complex. *J. Coord. Chem.* **2021**, *74*, 584-597, https://doi.org/10.1080/00958972.2021.1880574.
29. Góger, S.; Sandonas, L.M.; Müller, C.; Tkatchenko, A. Data-driven tailoring of molecular dipole polarizability and frontier orbital energies in chemical compound space. *Phys. Chem. Chem. Phys.* **2023**, *25*, 22211-22222, https://doi.org/10.1039/D3CP02256K.
30. Rijal, R.; Sah, M.; Lamichhane, H.P. Molecular simulation, vibrational spectroscopy and global reactivity descriptors of pseudoephedrine molecule in different phases and states. *Heliyon* **2023**, *9*, e14801, https://doi.org/10.1016/j.heliyon.2023.e14801.
31. Dege, N.; Gökce, H.; Doğan, O.E.; Alpaslan, G.; Ağar, T.; Muthu, S.; Sert, Y. Quantum computational, spectroscopic investigations on N-(2-((2-chloro-4,5-dicyanophenyl)amino)ethyl)-4-methylbenzenesulfonamide by DFT/TD-DFT with different solvents, molecular docking and drug-likeness researches. *Colloids Surf. A: Physicochem. Eng. Asp.* **2022**, *638*, 128311, https://doi.org/10.1016/j.colsurfa.2022.128311.
32. Koopmans, T Über die Zuordnung von Wellenfunktionen und Eigenwerten zu den Einzelnen Elektronen Eines Atoms. *Physica* **1934**, *1*, 104-113, https://doi.org/10.1016/S0031-8914(34)90011-2.
33. Vishwakarma, P.K.; Jaget, P.S.; Parte, M.K.; Maurya, R.C.; Rajak, D.K.; Chanpuria, A.; Shukla, A.; Ali, A. Experimental and theoretical evaluation of N-pyridoxal-salicylic acid hydrazide derived copper(II) complex with 2-methylimidazole. *J. Biomol. Struct. Dyn.* **2023**, *41*, 5305-5316, https://doi.org/10.1080/07391102.2022.2085801.
34. Pearson, R.G. The principle of maximum hardness. *Acc. Chem. Res.* **1993**, *26*, 250-255, https://doi.org/10.1021/ar00029a004.
35. Mulliken, R.S. Electronic Population Analysis on LCAO–MO Molecular Wave Functions. II. Overlap Populations, Bond Orders, and Covalent Bond Energies. *J. Chem. Phys.* **1955**, *23*, 1841-1846, https://doi.org/10.1063/1.1740589.
36. Korb, O.; Stützle, T.; Exner, T.E. Empirical Scoring Functions for Advanced Protein−Ligand Docking with PLANTS. *J. Chem. Inf. Model.* **2009**, *49*, 84-96, https://doi.org/10.1021/ci800298z.
37. Balouiri, M.; Sadiki, M.; Ibnsouda, S.K. Methods for *in vitro* evaluating antimicrobial activity: A review. *J. Pharm. Anal.* **2016**, *6*, 71-79, https://doi.org/10.1016/j.jpha.2015.11.005.
38. Sharma, B.; Shukla, S.; Rattan, R.; Fatima, M.; Goel, M.; Bhat, M.; Dutta, S.; Ranjan, R.K.; Sharma, M. Antimicrobial Agents Based on Metal Complexes: Present Situation and Future Prospects. *Int. J. Biomater.* **2022**, *2022*, 6819080, https://doi.org/10.1155/2022/6819080.

Supplementary materials

Table S1. Electronic spectral data of the synthesized complexes.

Complexes	λ_{max} (nm)	ν (cm^{-1})	ε ($L\ mol^{-1}\ cm^{-1}$)	Peak Assignment
[VO(ka)(macac)(H_2O)] C1	287	34843	1961	Charge transfer spectra
	300	33333	0458	Charge transfer spectra
	393	25445	0247	Charge transfer spectra
[VO(ka)(eacac)(H_2O)] C2	279	35842	2855	Charge transfer spectra
	307	32573	2852	Charge transfer spectra
	446	22422	0092	$b_2 \rightarrow a_1^*$
	571	17513	0160	$b_2 \rightarrow a_1^*$
[VO(ka)(dbm)(H_2O)] C3	289	34602	2702	Charge transfer spectra
	316	31646	2838	Charge transfer spectra
	361	27701	3013	Charge transfer spectra
	405	24691	2700	$b_2 \rightarrow a_1^*$
	485	20619	0215	$b_2 \rightarrow a_1^*$
[VO(ka)(bac)(H_2O)] C4	270	37037	1693	Charge transfer spectra
	438	22831	0078	$b_2 \rightarrow a_1^*$
	460	21739	0033	$b_2 \rightarrow a_1^*$

Table S2. Absolute electronegativity (χ_{abs}) and absolute hardness (η) electrophilicity index (ω), global softness (S) of kojic acid and **C2**.

Compounds	χ_{abs}	η	ω	S
kojic acid	-3.7967	-2.5779	-1.6847	-0.3879
[VO(ka)(eacac)(H_2O)]	-0.9441	-1.4851	-14.5455	-0.6734

Table S3. Representation data of Mulliken and NPA atomic charges of **C2**.

Atoms	Mulliken Analysis	NPA	Atoms	Mulliken Analysis	NPA
V(1)	0.0417	0.1118	O(20)	-0.2324	-0.2537
O(2)	-0.1834	-0.2139	H(21)	0.1779	0.1928
O(3)	-0.2196	-0.2599	C(22)	0.2249	0.3390
O(4)	-0.2054	-0.2478	C(23)	-0.1625	-0.2323
O(5)	-0.2147	-0.2633	H(24)	0.0803	0.0597
O(6)	-0.1079	-0.1862	C(25)	0.1468	0.2552
O(7)	-0.2637	-0.3335	C(26)	-0.2296	-0.2075
H(8)	0.2285	0.2604	H(27)	0.0843	0.0669
C(9)	-0.1191	-0.1618	H(28)	0.0885	0.0724
C(10)	0.1273	0.1995	H(29)	0.0957	0.0794
C(11)	0.0719	0.0914	O(30)	-0.1574	-0.1665
C(12)	-0.0134	0.0267	C(31)	-0.0406	0.0528
C(13)	0.1164	0.1726	H(32)	0.0884	0.0523
H(14)	0.1132	0.0880	H(33)	0.1061	0.0703
H(15)	0.1038	0.0619	C(34)	-0.2230	-0.1870
O(16)	-0.1204	-0.1070	H(35)	0.0839	0.0654
C(17)	-0.0548	0.0027	H(36)	0.0844	0.0671
H(18)	0.0835	0.0499	H(37)	0.0810	0.0624
H(19)	0.0846	0.0519	H(38)	0.2345	0.2673

Table S4. Calculated all (μ,β,α) components, (μ,α)-total and (β_0, $\Delta\alpha$) of **C2**.

	Kojic acid	C2		Kojic acid	C2
X	1.8705	3.5702	XXX	-8.0700	243.1519
Y	-2.7221	2.3257	YYY	-26.7453	27.8300
Z	-0.1568	5.0130	ZZZ	8.7077	49.0942

	Kojic acid	C2		Kojic acid	C2
μ Tot.	2.9472	6.5792	XYY	-3.7411	-18.9604
XX	-65.1101	-88.7723	XXY	-18.4990	29.2549
YY	-53.2055	-124.1600	XXZ	-2.7255	-14.1298
ZZ	-53.7255	-123.2983	XZZ	9.0287	-0.8001
XY	17.5333	0.9162	YZZ	0.7366	3.9440
XZ	0.1852	-6.8153	YYZ	0.8585	2.2987
YZ	0.4059	-3.0306	XYZ	6.0174	-3.3865
α	-57.3470	-112.0797	β_0	45.1162	234.5566
$\Delta\alpha$	11.6533	34.9648			

Table S5. The list of intermolecular interactions between the compounds docked with 2QBS.

Ligand	Score*	RMSD Å	Group interaction	Hydrogen Bond**	Bond Length Å
Co-crystallized	-78.21	0.42	ARG 47, ASP 48, VAL 49, LYS 120, TYR 46, ALA 217, SER 216, CYS 215, GLU 215, ARG 221, ILE 219, PRO 180, ASP 181, VAL 49, PHE 182, GLY 183, MET 258, GLN 266, ARG 254, ARG 24, GLN 262, GLY 259.	O sp^2 (O7)- O sp^3-TYR 46 O sp^2 (O7)-N sp^3-LYS 120 O sp^2 (O8)-N sp^3-LYS 120 O sp^2 (O28)-N sp^2- ARG 221 O sp^2 (O28)-N sp^2- ARG 221 O sp^2 (O28)-N sp^2 - GLN 266 O sp^2 (O28)-N sp^2 - PHE 182	3.078 3.125 2.900 3.060 3.032 2.897 2.746
Kojic acid	-39.68	0.01	LYS 120, TYR 46, ALA 217, SER 216, GLU 115, ARG 221, ILE 219, GLY 220, PRO 180, ASP 181, PHE 182, GLY 183, GLN 266, GLN 262, THR 263.	O sp^3(O1)-O sp^3- TYR 46 O sp^2(O2)-N sp^3- LYS 120 O sp^2(O2)-N sp^2- ARG 221 O sp^3(O4)-N sp^2 - PHE 182 O sp^3(O4)-N sp^2 - GLN 266	3.074 3.107 3.124 3.095 2,911
C1	-36.02	0.01	ARG 47, ASP 48, VAL 49, LYS 120, ARG 45, TYR 46, ALA 217, SER 216, ARG 221, ASP 181, VAL 49, PHE 182, GLN 262.	O sp^3(O17)-N sp^3-LYS 120 O sp^2(O16)-O sp^3TYR 46	2.904 3.075
C2	-39.26	0.53	ARG 47, ASP 48, VAL 49, LYS 120, TYR 46, ALA 217, SER 216, GLY 218, CYS 215, ARG 221, ILE 219, ASP 181, GLY 220, PHE 182, GLN 262, GLN 266.	O sp^3(O17)-N sp^2- ARG 47 O sp^3(O17)-O sp^2- ASP 48 O sp^2(O16)-N sp^2- ASP 48 O sp^2(O16)-N sp^2-ARG 47	3.066 3.197 2.925 3,322
C3	-57.22	0.20	ARG 47, ARG 45, ASP 48, VAL 49, LYS 120, TYR 46, ALA 217, SER 216, GLU 115, ARG 221, ILE 219, ASP 181, PHE 182, MET 258ARG 24, GLN 262, GLY 259.	O sp^3(O29)-O sp^2- GLN 262 O sp^3(O29)-N sp^2- GLN 262 O sp^3(O26)-O sp^2- ASP 48	2.978 2.933 3.187
C4	-47.85	0.06	ALA 27, ARG 47, ASP 48, VAL 49, LYS 120, TYR 46, ALA 217, SER 216, ARG 221, GLY 220, ILE 219, VAL 49, PHE 182, MET 258, ARG 254, ARG 24, TYR 20, LEU 260, GLN 262, GLY 259.	-	-

*The docking score ($PLANTS_{PLP}$ score) is a function.
** The numbering of the atoms was done according to the software Figure 12.

Table S6. *In silico* ADME properties of the compound **C1-C4.**

Parameters	C1	C2	C3	C4
MW(g/mol)	341.16	355.19	449.30	387.23

Parameters	C1	C2	C3	C4
heavy atoms	21	22	30	25
Aromatic heavy atoms	0	0	12	6
Fraction Csp3	0.27	0.33	0.05	0.12
Rotatable bonds	2	3	3	2
H-bond acceptors	9	9	8	8
H-bond donors	2	2	2	2
Molar Refractivity	61.09	65.90	100.38	79.91
TPSA (Å²)	117.59	117.59	108.36	108.36
Log P	-1.79	-1.51	0.23	-0.63
LogS	-1.24	-1.49	-3.93	-2.70
GI absorption	High	High	High	High
BBB permeant	No	No	No	No
P-gp substrate	No	No	Yes	Yes
CYP1A2	No	No	No	No
CYP2C19	No	No	No	No
CYP2C9	No	No	No	No
CYP2D6	No	No	No	No
CYP3A4	No	No	No	No
Log K_p cm/s	-9.04	-8.86	-7.68	-8.20
Bioavailability	0.56	0.56	0.56	0.56
Synthetic accessibility	4.56	4.65	4.90	4.63

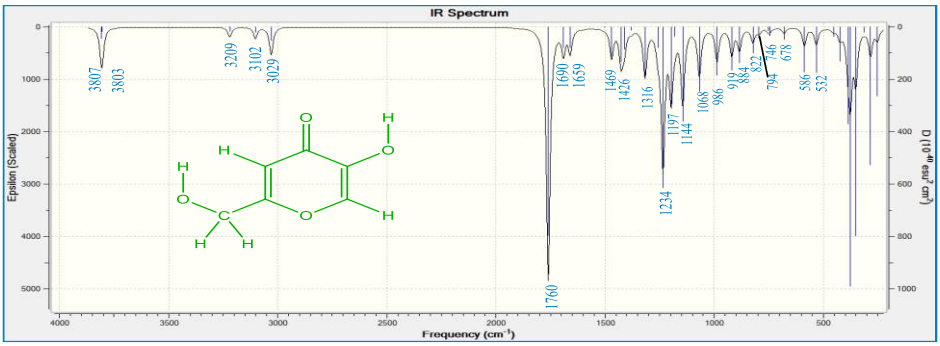

Figure S1. Theoretical IR spectrum of kojic acid.

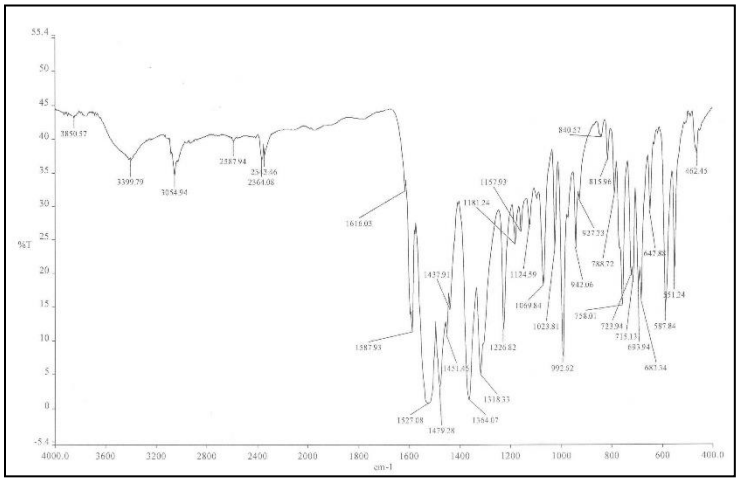

Figure S2. IR Spectrum of [VO(ka)(dbm)(H_2O] **C3.**

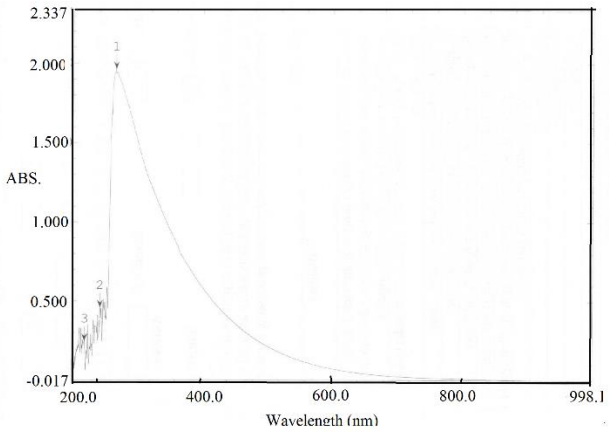

Figure S3. Electronic Spectrum of [VO(ka)(macac)(H_2O)] **C1.**

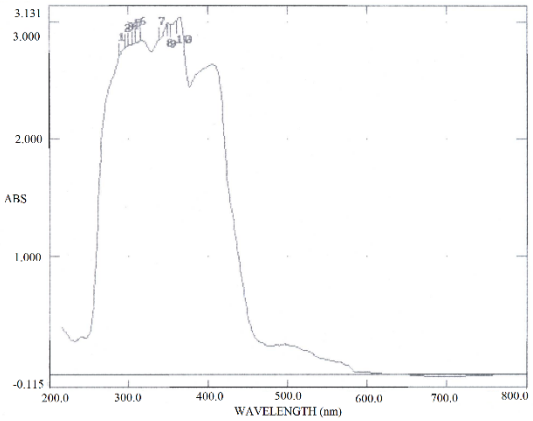

Figure S4. Electronic Spectrum of [VO(ka)(dbm)(H_2O)] **C3.**

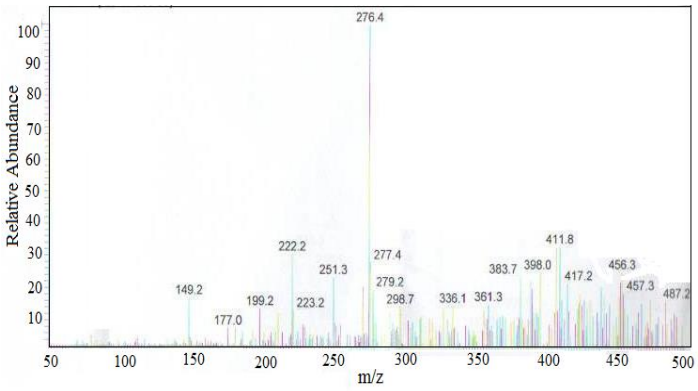

Figure S5. ESI-Mass Spectrum of [VO(ka)(macac)(H_2O] **C1.**

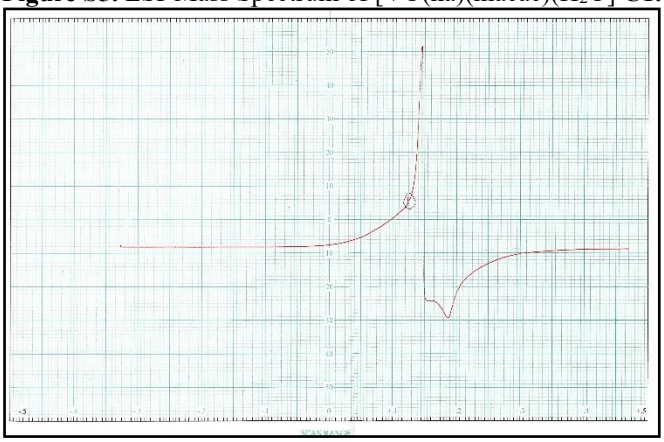

igure S6. ESR Spectrum of [VO(ka)(eacac)(H_2O] **C2**.

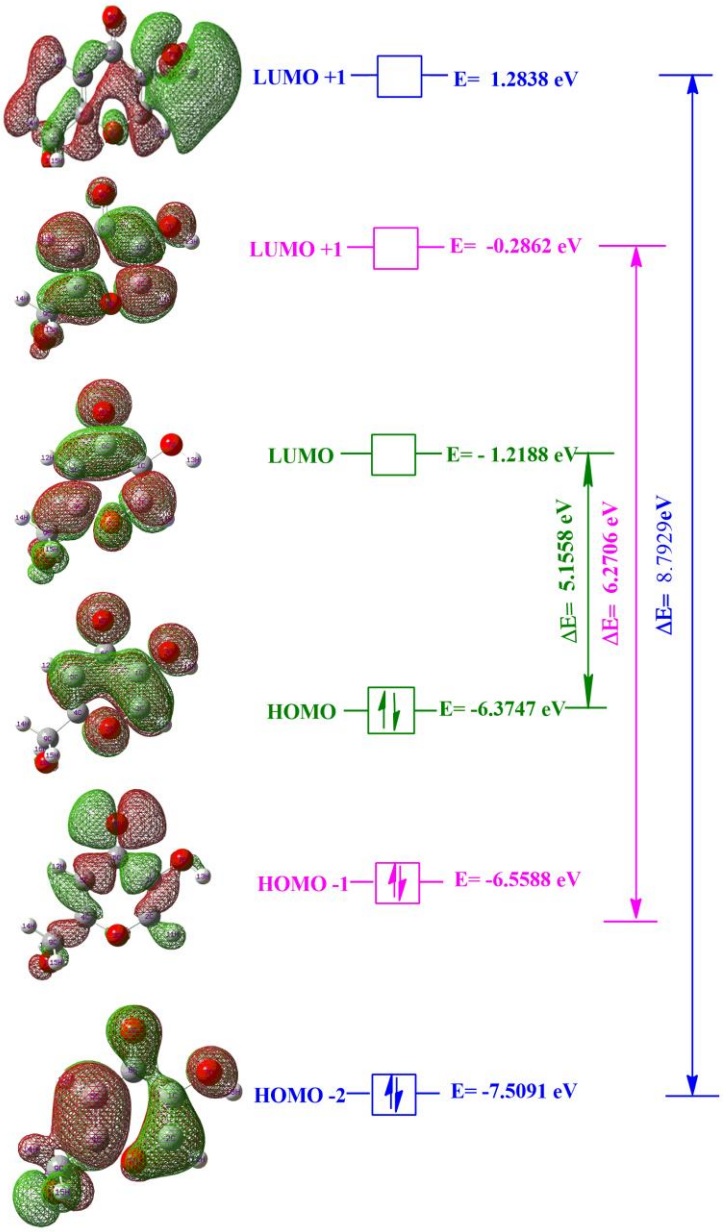

Figure S7. HOMO–LUMO Structure with energy level diagram of kojic acid.

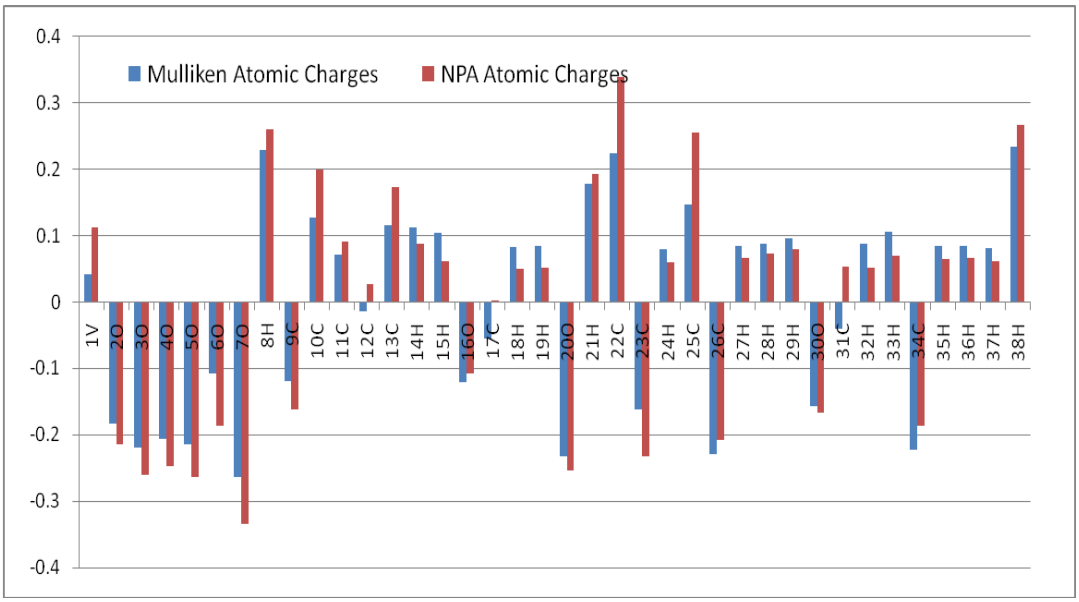

Figure S8. Graphical representation of Mulliken atomic charges and Natural Population Analysis of **C2**.

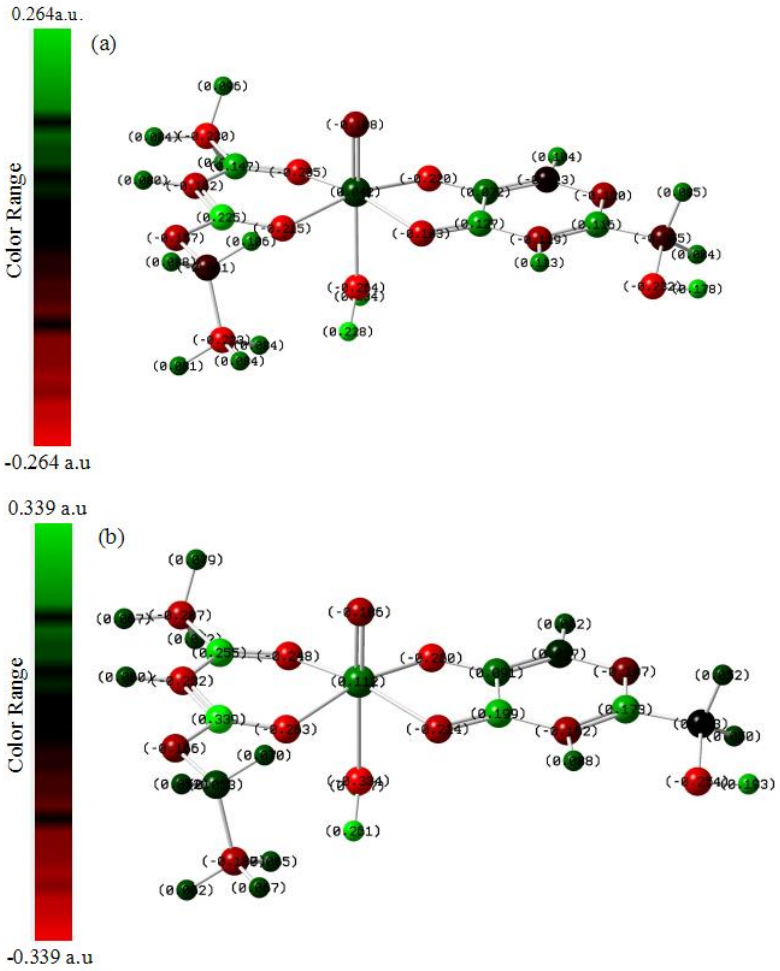

Figure S9. Structural representation of Mulliken atomic charges (a) and natural population analysis (b) of C2.

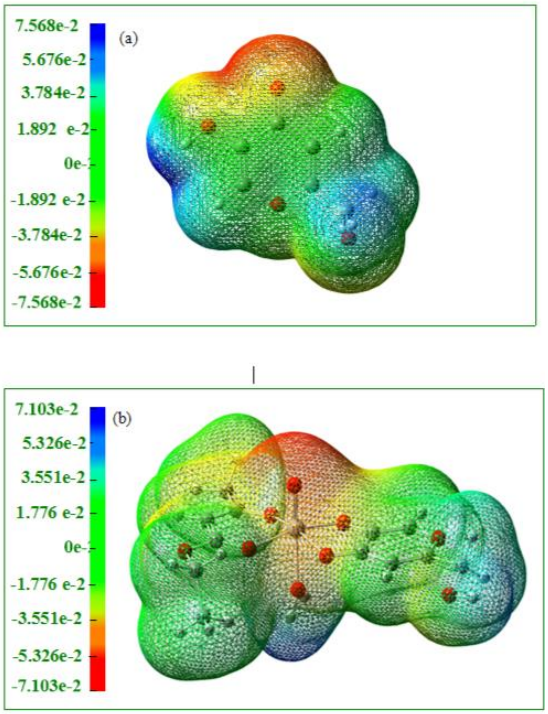

Figure S10. Molecular electrostatic potential (MESP) of (a) kojic acid and (b) C2 with color range, along with scale.

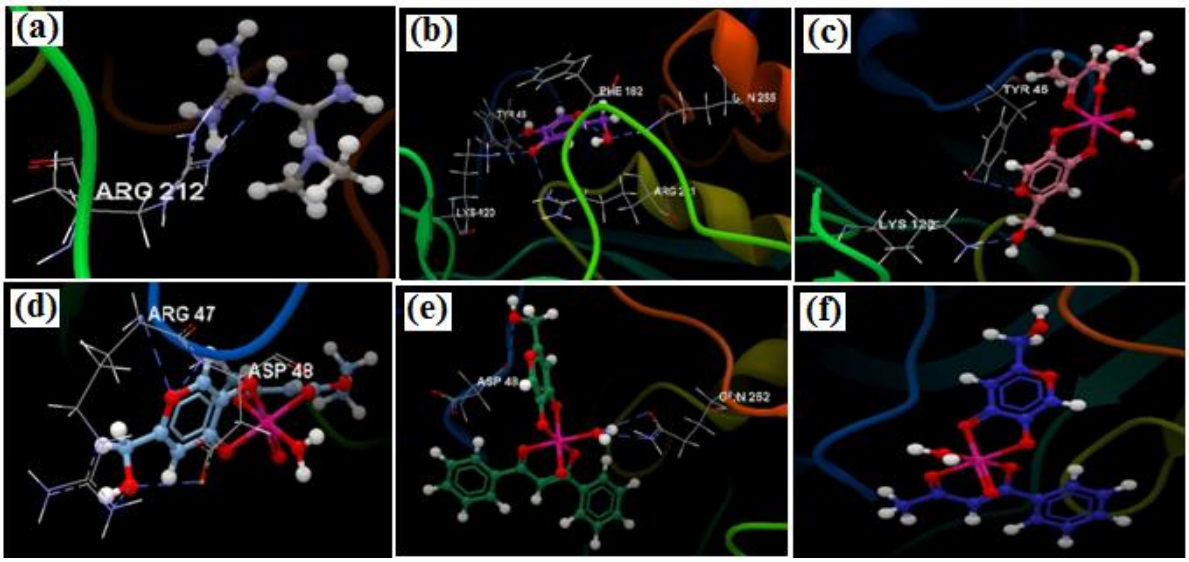

Figure S11. Hydrogen bond (blue dotted lines) between (a) co-crystallized (024) and TYR 46, LYS 120, ARG 221, PHE 182 and GLN 266 amino acids, (b) Kojic Acid and TYR 46, LYS 120, ARG 221, PHE 182 and GLN 266 amino acids, (c) C1 and TYR 46 and LYS 120 amino acids, (d) C2 and ARG 47and ASP 47 amino acids, (e) C3 and GLN 262 and ASP 48amino acids, (f) C4 (no hydrogen bonds).

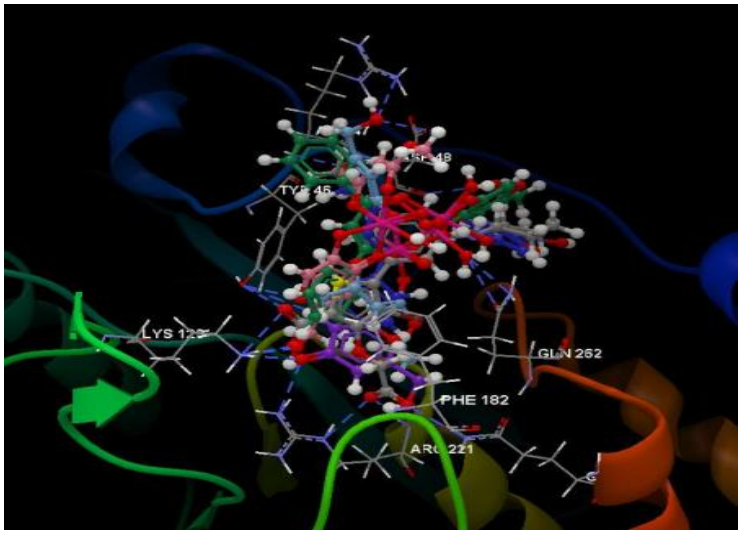

Figure S12. Docking pose of the co-crystallized, of the studied compounds in the binding site of 2QBS.

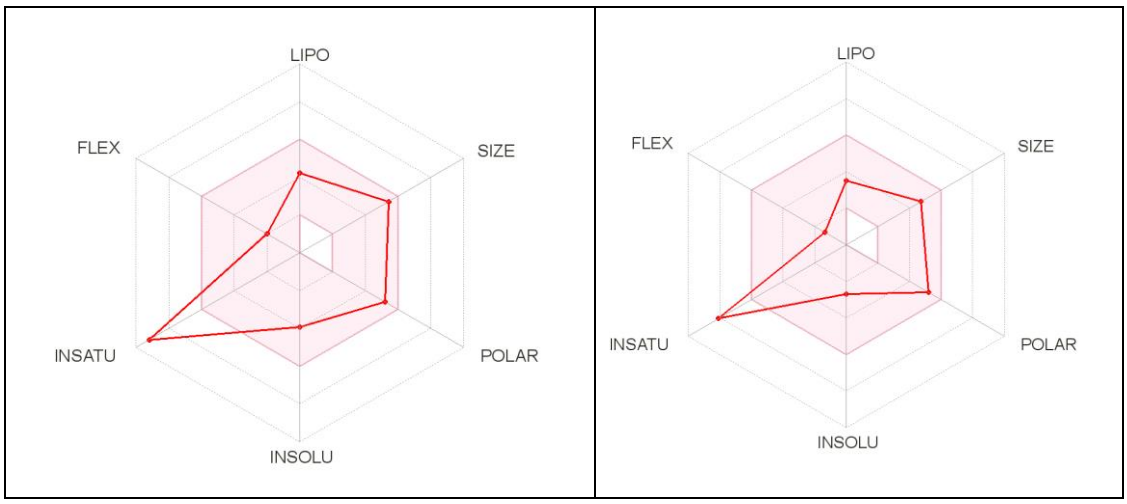

Figure S13. Insilico ADME egg models of **C1-C4.**

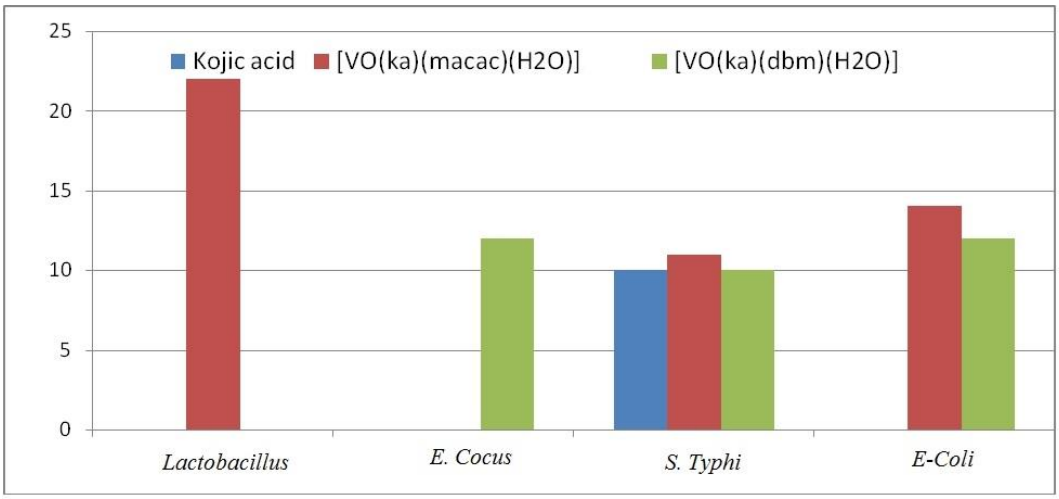

Figure S14. Antibacterial activity of kojic acid and two representative complexes.